An asteroseismic study of the β Cephei star 12 Lacertae: multisite spectroscopic observations, mode identification and seismic modelling

M. Desmet[1]$\star$, M. Briquet[1]$\dagger$, A. Thoul[2]$\ddagger$, W. Zima[1], P. De Cat[3], G. Handler[4], I. Ilyin[5], E. Kambe[6], J. Krzesinski[7], H. Lehmann[8], S. Masuda[9], P. Mathias[10], D. E. Mkrtichian[11], J. Telting[12], K. Uytterhoeven[13], S. L. S. Yang[14] and C. Aerts[1,15]

[1] *Institute of Astronomy - KULeuven, Celestijnenlaan 200D, 3001 Leuven, Belgium*
[2] *Institut d'Astrophysique et de Géophysique de l'Université de Liège, 17, Allée du 6 Août, 4000 Liège, Belgium*
[3] *Koninklijke Sterrenwacht van België, Ringlaan 3, 1180 Brussel, Belgium*
[4] *Institut für Astronomie, Universität Wien, Türkenschanzstrasse 17, 1180 Wien, Austria*
[5] *Astrophysical Institute Potsdam, An der Sternwarte 16 D-14482 Potsdam, Germany*
[6] *Okayama Astrophysical Observatory, National Astronomical Observatory, Kamogata, Okayama 719-0232, Japan*
[7] *Mt. Suhora Observatory, Cracow Pedagogical University, Ul. Podchorazych 2, 30-084 Cracow, Poland*
[8] *Karl-Schwarzschild-Observatorium, Thüringer Landessternwarte, 7778 Tautenburg, Germany*
[9] *Tokushima Science Museum, Asutamu Land Tokushima, 45 - 22 Kibigadani, Nato, Itano-cho, Itano-gun, Tokushima 779-0111, Japan*
[10] *UNS, CNRS, OCA, Campus Valrose, UMR 6525 H. Fizeau, F-06108 Nice Cedex 2, France*
[11] *Astronomical Observatory of Odessa National University, Marazlievskaya, 1v, 65014 Odessa, Ukraine*
[12] *Nordic Optical Telescope, Apartado 474, 38700 Santa Cruz de La Palma, Spain*
[13] *Instituto de Astrofísica de Canarias, Calle Via Láctea s/n, 38205 La Laguna (TF, Spain)*
[14] *Department of Physics and Astronomy, Universtity of Victoria, Victoria, BC V8W 3P6, Canada*
[15] *Department of Astrophysics, University of Nijmegen, PO Box 9010, 6500 GL Nijmegen, The Netherlands*

ABSTRACT

We present the results of a spectroscopic multisite campaign for the β Cephei star 12 (DD) Lacertae. Our study is based on more than thousand high-resolution high S/N spectra gathered with 8 different telescopes in a time span of 11 months. In addition we make use of numerous archival spectroscopic measurements. We confirm 10 independent frequencies recently discovered from photometry, as well as harmonics and combination frequencies. In particular, the SPB-like g-mode with frequency $0.3428\,\mathrm{d}^{-1}$ reported before is detected in our spectroscopy. We identify the four main modes as $(l_1, m_1) = (1, 1)$, $(l_2, m_2) = (0, 0)$, $(l_3, m_3) = (1, 0)$ and $(l_4, m_4) = (2, 1)$ for $f_1 = 5.178964\,\mathrm{d}^{-1}$, $f_2 = 5.334224\,\mathrm{d}^{-1}$, $f_3 = 5.066316\,\mathrm{d}^{-1}$ and $f_4 = 5.490133\,\mathrm{d}^{-1}$, respectively. Our seismic modelling shows that f_2 is likely the radial first overtone and that the core overshooting parameter α_{ov} is lower than 0.4 local pressure scale heights.

Key words: stars: main-sequence – stars: individual: 12 Lac – stars: oscillations – stars: interiors

1 INTRODUCTION

12 (DD) Lacertae (12 Lac) is one of the best observed β Cephei stars, a class of variable early B-type stars whose light and radial velocity changes are due to gravity and pressure-mode pulsations of low radial order (Stankov & Handler 2005). The variability of 12 Lac has been known for one century during which the star has been extensively studied. We refer to Handler et al. (2006) for a very detailed summary of the work accomplished in the past.

Despite the numerous earlier studies, safe mode identification of the observed modes was not achieved until recently. Thanks to an intensive photometric multisite campaign, Handler et al. (2006) unambiguously iden-

---

$\star$ E-mail:maarten.desmet@ster.kuleuven.be
$\dagger$ Postdoctoral Fellow of the Fund for Scientific Research, Flanders
$\ddagger$ Chercheur Qualifié au Fonds National de la Recherche Scientifique, Belgium.
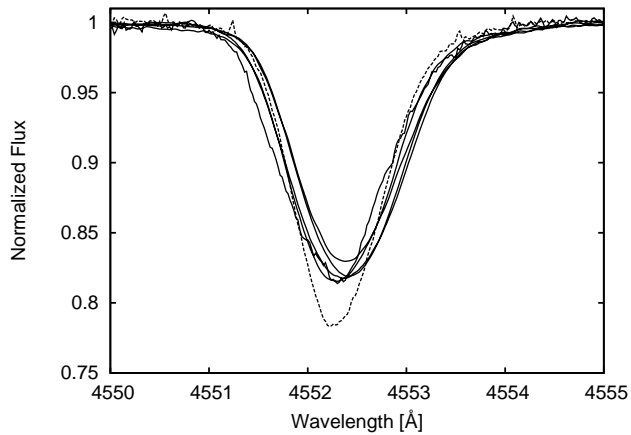
Figure 1. The average profiles of the Si III $\lambda4553$ Å line from each observatory. The dashed line shows the average profile from the BAO observatory. This profile deviates from all the others because the relatively small number of spectra implies that the beat cycle is not well covered (see Table 1).
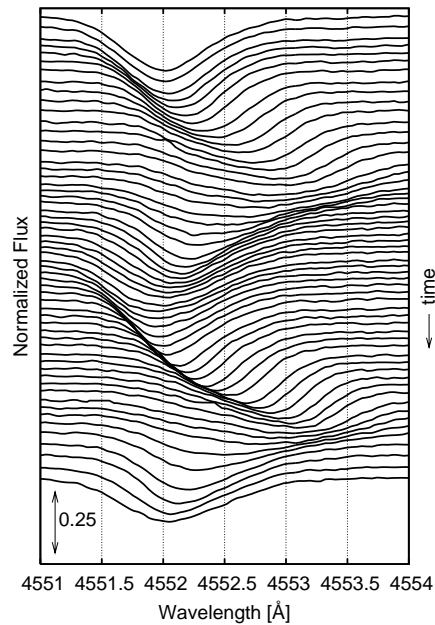

Figure 2. The Si III line profiles of 1 night (JD 2452898) taken with the McDonald telescope. The arrow indicates the flux scale of one spectrum.

tified the ℓ-values of the five modes with the highest photometric amplitudes. In addition, they found constraints on ℓ for the six other independent modes detected in their dataset. Their ℓ-identifications ruled out the assumption previously adopted for stellar modelling (e.g. Dziembowski & Jerzykiewicz 1999) that three of the strongest modes, almost equidistant, belong to the same multiplet. Indeed, these three modes are actually associated to three different values of the degree ℓ.

Obviously, reliable empirical mode identification was indispensable before any attempt of in-depth seismic modelling of 12 Lac. To complement the photometric results, a spectroscopic multisite campaign has also been devoted to the star. The additional constraints are presented in this paper. They mainly concern the identification of m-values for the strongest modes and the derivation of the stellar equatorial velocity. A detailed abundance analysis of 12 Lac was already presented in Morel et al. (2006), showing that the abundances of all considered chemical elements are indistinguishable from the values found for OB dwarfs in the solar neighbourhood.

Besides our line-profile study, we also describe a detailed stellar modelling based on all available observational results, state-of-the-art numerical tools and up-to-date physical inputs appropriate to model β Cephei stars, as explained in detail in Miglio (2007). Dziembowski & Pamyatnykh (2008) already computed models for 12 Lac, making some assumptions and restrictions not supported by our study. In the present paper, we discuss our conclusions which differ from those of Dziembowski & Pamyatnykh (2008).

2   OBSERVATIONS AND DATA REDUCTION

The data originate from a spectroscopic multisite campaign dedicated to our studied star. In addition, we added the 903 spectra of Mathias et al. (1994), which allowed us to increase the time span and, thus, to achieve a better frequency accuracy. In total 1820 observations were gathered using 9 different small- to medium-sized telescopes spread over the northern continents. Table 1 summarizes the logbook of our spectroscopic data. The resolution $(\lambda/\Delta\lambda)$ of the instruments ranged from 30 000 to 80 000 and the average S/N ratio near 4500 Å between 180 and 380.

All data were subjected to the normal reduction process, which consists of de-biasing, background subtraction, flat-fielding and wavelength calibration . Finally, the heliocentric corrections were computed, and all spectra were normalized to the continuum by fitting a cubic spline function.

For our study, we considered the Si III triplet around 4567 Å because its characteristics simplify the modelling of the line-profile variations, which we use for mode identification. Indeed, these silicon lines are sufficiently strong without being much affected by blending. Moreover, they are dominated by temperature broadening, such that the intrinsic profile can simply be modelled with a gaussian. Finally, they are not too sensitive to temperature variations (see De Ridder et al. 2002; Aerts & De Cat 2003), so that neglecting them remains justified.

The similar average radial velocity of about $-15\,\mathrm{km\,s^{-1}}$ for 1990-1992, 2003-2004 and earlier measurements (e.g. Wilson 1953) definitely excludes the possibility of 12 Lac being a spectroscopic binary. Besides the pulsation effect, the different centroids are due to the different zero points of the different telescopes. Before extracting the pulsation information from the whole dataset, it is necessary to correct for this effect. The spectra were shifted in such a way that the constant of a least-squares sine fit using the first three dominant modes is put to the same value for each observatory.

In Fig. 1 we superimpose the average profiles of the Si III $\lambda4553$ Å line computed for each observatory separately, after correction for the different zero points. We note that the centroid of the lines are in good agreement but not exactly
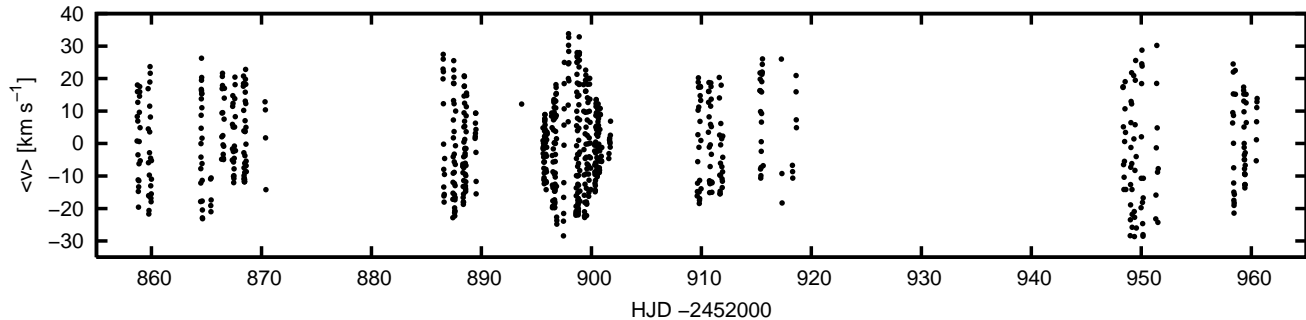
Figure 3. The densest part of the time series of the Si III radial velocities ($\langle v^1 \rangle$) of 12 Lac derived from each spectrum taken during the dedicated multisite campaign (7 Aug. 2003 – 17 Nov. 2003).

Table 1. Log of our spectroscopic multisite campaign. The Julian Dates are given in days, ΔT denotes the time-span expressed in days, N is the number of spectra and S/N denotes the average signal-to-noise ratio for each observatory measured at the continuum between 4500 and 4551 Å.

Observatory (Name of the instrument; resolution)	Long.	Lat.	Telescope	Julian Date Begin	End	ΔT	N	S/N	Observer(s)
2003-2004				-2450000					
Apache Point Observatory (ARC; 31500)	$-105°49'$	$+32°46'$	3.5-m	2927	2928	2	93	300	JK
Bohyunsan Astronomical Observatory (BOES; 30000)	$+128°58'$	$+36°09'$	1.9-m	3109	3109	1	27	180	DM
Dominion Astrophysical Observatory (45000)	$-123°25'$	$+48°31'$	1.2-m	2858	2859	2	66	250	SY
				2909	2911	3	42		
McDonald Observatory (Sandiford; 60000)	$-104°01'$	$+30°40'$	2.1-m	2893	2901	9	210	380	GH
			2.7-m	3195	3198	4	31	350	GH
Nordic Optical Telescope (SOFIN; 80000)	$-17°53'$	$+28°45'$	2.6-m	2947	2951	5	32	370	KU, JT, II
				2957	2960	4	47		
Okayama Astrophysical Observatory (HIDES; 685000)	$+133°35'$	$+34°34'$	1.88-m	3201	3202	2	7	180	SM
				3205	3205	1	6		
				3208	3210	3	17		
Thüringer Landessternwarte Tautenburg (67000)	$+11°42'$	$+50°58'$	2-m	2863	2869	7	103	240	HL
				2886	2889	4	100		
				2895	2900	6	105		
				2914	2918	5	31		
1990-1992				-2440000					
Observatoire de Haute-Provence (AURELIE; 42000)	$+5°42'$	$+43°55'$	1.52-m	8135	8135	1	70	220	PM
				8224	8224	1	52		
				8227	8227	1	35		
				8845	8858	14	582		
				8884	8889	6	164		
Total						82	1820		

at the same position. Larger differences can be seen for the width and the depth of the lines. Such deviant average profiles are due to the limited time spread of the observations together with the multiperiodic character of the pulsations. In the case of a similar spectroscopic multisite campaign devoted to ν Eridani, Aerts et al. (2004) observed similar differences, which are not caused by instrumental and/or signal-to-noise ratio effects.

Fig. 2 displays the large and complex radial-velocity variations of 12 Lac. The plotted spectra were taken with

the McDonald telescope during only one night. In Fig. 3, we show the radial velocities for the densest part of the multisite campaign (7 Aug. 2003 – 17 Nov. 2003). A clear beating pattern is seen.

3 FREQUENCY ANALYSIS

We performed a frequency analysis on the first three velocity moments $\langle v^1 \rangle$, $\langle v^2 \rangle$ and $\langle v^3 \rangle$ (see Aerts et al. 1992,

Table 2. Frequencies and radial velocity amplitudes of the first moment of the Si III $\lambda 4553$ Å line together with their S/N ratio (we refer to the text for explanation). Error estimates (Montgomery & O'Donoghue 1999) for the independent frequencies range from $\pm 0.000002\,\mathrm{d}^{-1}$ for f_1 to $\pm 0.00002\,\mathrm{d}^{-1}$ for f_9. The error on the amplitude is $0.01\,\mathrm{km\,s}^{-1}$.

ID	Frequency		Amplitude in $\langle v^1 \rangle$	S/N
	$[\mathrm{d}^{-1}]$	$[\mu\mathrm{Hz}]$	$[\mathrm{km\,s}^{-1}]$	
f_1	5.178964	59.941713	14.50	99.6
f_2	5.334224	61.738704	7.70	52.2
f_3	5.066316	58.637917	6.26	42.7
f_4	5.490133	63.543206	2.61	17.5
f_g	0.342841	3.968067	1.34	7.1
f_5	4.241787	49.09475	0.91	6.7
f_6	5.218075	60.394387	0.84	5.8
f_7	6.702318	77.573125	0.62	4.4
f_8	7.407162	85.731042	0.67	4.9
f_9	5.84511	67.65184	0.79	5.2
$2f_1$	10.35814	119.88590	0.63	4.5
$f_2 + f_3$	10.40056	120.37693	0.72	3.8
$f_1 + f_2$	10.51319	121.68044	2.59	19.7
$2f_1 + f_3$	15.42400	178.51860	0.72	6.6
$f_1 + f_2 + f_3$	15.57950	180.31838	0.71	6.4

for a definition of the moments of a line profile) of the Si III $\lambda 4553$ Å line by means of the program Period04 (Lenz & Breger 2005). For some β Cephei stars (see Telting et al. 1997; Schrijvers et al. 2004; Briquet et al. 2005) a two-dimensional frequency analysis on the spectral lines led to additional frequencies compared to a one-dimensional frequency search in the moments. For 12 Lac 1D analysis on $\langle v^2 \rangle$ and $\langle v^3 \rangle$ did not reveal additional independent periodicities compared to those present in the first moment. We also do not find additional frequencies in the 2D frequency analysis. The 2D analysis is more sensitive to the detection of high-degree modes than a 1D analysis so here we have already an indication that the frequencies are low-degree modes.

In what follows we only describe our frequency analysis on $\langle v^1 \rangle$, which is the radial velocity from which the fitted averaged radial velocity is subtracted.

The frequencies were determined with the standard method of prewhitening the data. In addition we made use of a procedure available in Period04 which allows to improve the detected frequency from non-linear least-squares fitting with the maxima in the Fourier transform as starting values. At each step of prewhitening we subtracted a theoretical multi-sine fit with the amplitudes, phases and also optimized frequencies that yielded the smallest residual variance. All peaks exceeding an amplitude signal-to-noise ratio above 4 in the Fourier periodogram (Breger et al. 1993, 1999) were retained. The noise level was calculated from the average amplitude, computed from the residuals, in a $2\,\mathrm{d}^{-1}$ interval centered on the frequency of interest.

The detected frequencies are listed in Table 2 and the Fourier periodograms are shown in Fig. 4. Our frequency analysis reaffirmes the presence of the already well-known 5 main frequencies (Mathias et al. 1994) together with the new independent signals and combination frequencies discovered by Handler et al. (2006). We note that one addi-

tional independent frequency ($f_p = 5.30912\,\mathrm{d}^{-1}$) was found by the latter authors and not by us. An important result is that we clearly recover the low-frequency signal possibly originating from a g-mode. Such a SPB-like oscillation does not seem to be uncommon among β Cephei stars. For instance, it was also observed in 19 Mon (Balona et al. 2002), in ν Eridani (Handler et al. 2004), in δ Ceti (Aerts et al. 2006) and in V1449 Aql (Briquet et al., in preparation). We also point out that such hybrid SPB-β Cep pulsators are theoretically predicted for hotter stars than previously thought (Miglio et al. 2007 versus Pamyatnykh 1999).

The equivalent width (EW) of the silicon line of 12 Lac clearly varies with the two dominant modes f_1 and f_2. The sum frequency $f_1 + f_2$ is even present. Fig. 5 represents phase diagrams for both frequencies. Such a strong EW variability of 9% is generally not observed in pulsating B-type stars. Indeed, typical relative EW peak-to-peak amplitudes are of the order of a few percent (De Ridder et al. 2002; De Cat & Aerts 2002). However, for several β Cephei stars, one clear sinusoidal variation is observed in their EW, with the same frequency as in the radial velocity. The known cases are targets pulsating multiperiodically with a high-amplitude dominant radial mode, such as δ Ceti (Aerts et al. 1992), ν Eridani (Aerts et al. 2004) and V1449 Aql (Briquet et al., in preparation). In the case of 12 Lac, we note that the EW signal is multiperiodic with a dominant $(1, 1)$-mode, followed by a radial mode of lower amplitude (see next section). For the four strongest modes, the frequency values derived from our spectroscopic measurements are exactly the same, within the errors, as the photometric ones by Handler et al. (2006). For the modes with radial velocity amplitudes typically lower than $1\,\mathrm{km\,s}^{-1}$, there are differences between values derived from both kinds of data, which might have some influence on the mode identification outcome. Because the number of observations as well as the time span of the datasets in the literature are much larger than the dedicated spectroscopic ones, the literature frequency values are expected to be more accurate and hence we adopt them.

4 MODE IDENTIFICATION

4.1 The methods used

We used two different and independent methods to identify the modes, namely the moment method (Briquet & Aerts 2003) and of the Fourier parameter fit method (FPF method, Zima 2006).

The basic principles of both methods are the following. With the moment method the wavenumbers (l, m) and the other continuous velocity parameters are determined in such a way that the theoretically computed first three moment variations of a line profile best fit the observed ones. In the FPF method, for every detected pulsation frequency, the zero point, amplitude, and phase are computed for every wavelength bin across the profile by a multi-periodic least-square fit. Subsequently the zero-point profile, the amplitude and the phase values across the profile are fitted with theoretical values derived from synthetic line profiles. The first technique has the advantage to be less computationally demanding, allowing to test a huge grid for (ℓ, m) and for the other parameters. Moreover, the modes are deter-
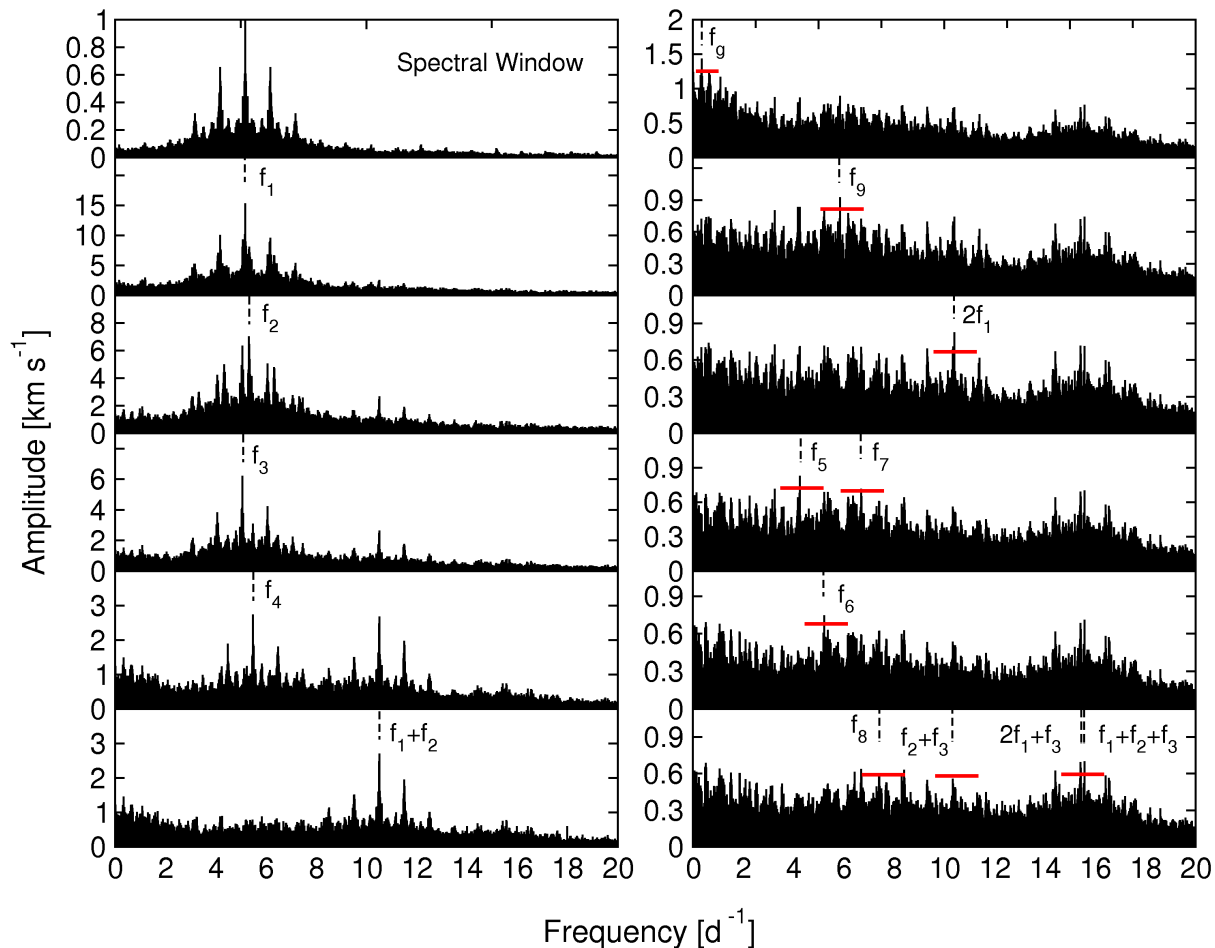
Figure 4. Amplitude spectra of 12 Lac computed from the first moment of the Si III λ4553 Å line. The uppermost panel shows the spectral window of the data. All subsequent panels show the periodograms in different stages of prewhitening. The significance limit in red is calculated according to 4 times the noise over a $2\,\mathrm{d}^{-1}$-range around the significant frequency.

mined simultaneously by fitting a multiperiodic signal taking into account the coupling terms appearing in the second and third moments. For the second technique, the fitting is carried out by applying genetic optimization routines in a large parameter space and mono-mode fits are used in order to speed up the computations. Once the best solutions are constrained, a multi-mode fit is performed. The strength of the FPF method is its ability to estimate the significance of the derived mode parameters by means of a χ^2 test (all χ^2-values listed in the text are reduced χ^2 values, see Zima 2008).

The FPF method is not optimally suited to study high-amplitude modes, but as described further, the application of the FPF method for 12 Lac proved to be succesful. As shown by Zima et al. (2004) and by Zima (2006), both mode identification techniques constrain the value of the azimuthal number m better than the degree ℓ for low $v \sin i$. Since the photometric data provided us with unambiguous ł-values for the 5 main modes (Handler et al. 2006), a valid strategy is to make use of spectroscopy to identify the values of m, adopting the ł-values obtained from photometry.
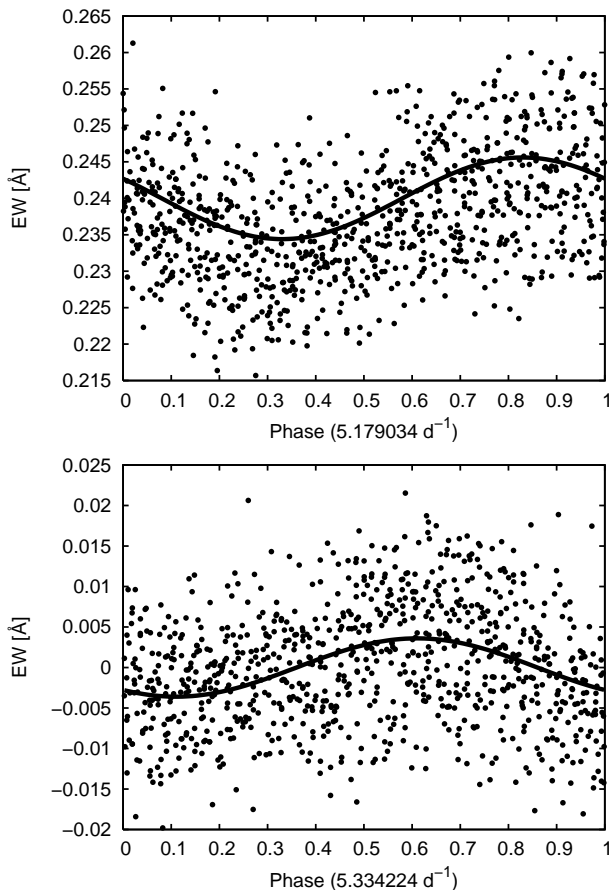
Such a methodology already proved to be successful for two other β Cephei stars (Briquet et al. 2005; Mazumdar et al. 2006). Mode identification results have been obtained with the software package FAMIAS[1] (Zima 2008).

In what follows we present in detail our mode identification by the FPF method. The moment method gave compatible results, but did not give additional constraints on the (ℓ, m) than the ones we present here. Both techniques found the same m-values for the three main modes, giving us much confidence in our outcome. For the fourth mode, the moment method derived the sign of m in agreement with the FPF method, which could further constrain its value.

4.2 Derivation of the wavenumbers

For the FPF method, a sophisticated theoretical formalism for the modelling of the displacement field is used and in-
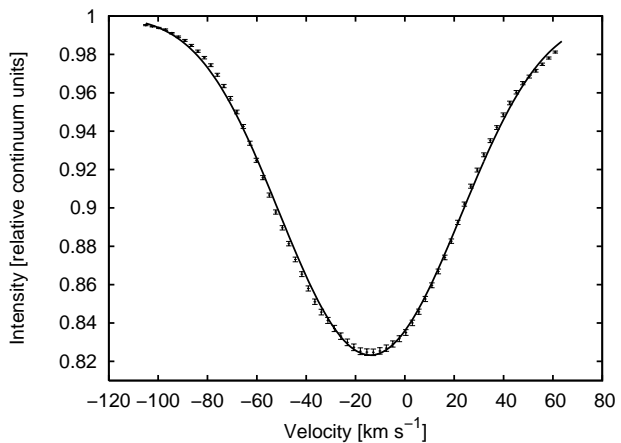
---

[1] FAMIAS has been developed in the framework of the FP6 European Coordination Action HELAS - `http://www.helas-eu.org/`.

Figure 6. Observed zero-point profile (points) and best fit when taking into account the four main modes (solid line) by means of a synthetic rotationally broadened profile ($v \sin i = 36.7 \, \mathrm{km \, s^{-1}}$, W=15.3 $\mathrm{km \, s^{-1}}$, $\sigma = 22.1 \, \mathrm{km \, s^{-1}}$).

Figure 5. Phase diagrams of the equivalent width of the Si III λ4553 Å line, for f_1 (top panel), and for f_2 (bottom panel) after prewhitening with f_1.

cludes, for instance, first-order effects of the Coriolis force as well as temperature variations of the stellar atmosphere. We refer to Zima (2006, 2008) for details on the computation of the synthetic line-profile variations. The fixed parameters are the mass and the radius. When taking into account temperature effects, the effective temperature T_{eff} and the logarithm of the gravity $\log g$ have also to be fixed. For 12 Lac, we adopted the values $M = 13.5 \, M_{\odot}$ (Handler et al. 2006), $R = 6.9 \, R_{\odot}$ (Handler et al. 2006), $T_{\mathrm{eff}} = 24500 \pm 1000$ K (Morel et al. 2006), $\log g = 3.65 \pm 0.15$ (Morel et al. 2006). We note that the mode identification results are robust when using different values for these parameters, within the errors.

In a first step we identified the 3 main modes ($f_{1,3,4}$) by fitting mono-mode Fourier parameters, which are computed from synthetic line profiles evenly sampled over one pulsation cycle (for more explanations see Zima 2006). Moreover, we neglected the equivalent width variations of the spectral line due to temperature variations. In order to restrict the parameter space, we estimate roughly the values of the projected rotational velocity $v \sin i$, the width of the intrinsic gaussian profile σ, and the equivalent width W from a least-squares fit of a rotationally broadened synthetic profile to the zero-point profile. This gives only a crude estimate of these three parameters, because the pulsational broadening is ignored in this fit, but it serves the purpose of defin-

ing our appropriate grid. Moreover $v \sin i$ will be overestimated. When taken into account the pulsational broadening caused by the four main modes we acquire a $v \sin i$ of $36.7 \, \mathrm{km \, s^{-1}}$ (see Fig. 6). A genetic optimization with the following free parameters was afterwards adopted: $\ell \in [0, 4]$ with a step of 1, $m \in [-\ell, \ell]$ with a step of 1, the surface velocity amplitude $a \in [10, 110] \, \mathrm{km \, s^{-1}}$ with a step of $1 \, \mathrm{km \, s^{-1}}$, the stellar inclination angle $i \in [5, 85]\,^{\circ}$ with a step of $5\,^{\circ}$, $v \sin i \in [20, 48] \, \mathrm{km \, s^{-1}}$ with a step of $0.5 \, \mathrm{km \, s^{-1}}$ and $\sigma \in [10, 30] \, \mathrm{km \, s^{-1}}$ with a step of $0.1 \, \mathrm{km \, s^{-1}}$. We fixed f_2 as a radial mode and only fitted the continuous parameters for that mode.

In Table 3, the 5 best solutions from a fit to the Fourier parameters are listed for each frequency. The 95%-confidence limit of χ^2 is 1.15. The most probable solutions are $(l_1, m_1) = (1, 1)$, $(l_3, m_3) = (1, 0)$ and $(l_4, m_4) = (2, 1)$ (where a positive m-value denotes a prograde mode). We point out that the agreement between theory and observations is not perfect. More precisely, the observed asymmetry with respect to the centroid of the amplitudes across the line of the dominant modes is not completely reproduced by our model. Such an asymmetry can be caused by EW variations of the intrinsic line profile due to local temperature variations (Schrijvers & Telting 1999). We considered EW variations in our fitting procedure but we did not obtain an improved solution compared to the case of a constant EW.

In a second step we attempted to improve the solutions by simultaneously fitting the four main modes and using all the original data points. This however was computationally not possible. To restrict the computation time we took a subset of our complete time series. Our subset resulted in 388 spectra with a time span of 4 months. We also fixed the wave numbers according to our mono-mode fit described above. We succeeded in improving the surface velocity amplitudes together with the inclination, $v \sin i$ and the width of the intrinsic profile. The χ^2 values are lower than in the mono-mode fit and we are able to reproduce part of the asymmetry in the amplitude across the line as explained above (see Ta-

Table 3. Mode parameters derived from the FPF mono-mode method. For each pulsation mode, the five best solutions are shown together with the second best (ℓ, m) identifications. For f_5 we list the different solutions for m. a_s is the surface velocity amplitude (km s^{-1}); i is the stellar inclination angle in degrees; $v \sin i$ is the projected rotational velocity, σ is the width of the intrinsic profile, both expressed in km s^{-1}. Due to spherical symmetry we have not indicated the inclination angle for radial modes. The 95% significance limit is at $\chi^2 = 1.15$.

χ^2	ł	m	a_s [km s^{-1}]	i [°]	$v \sin i$ [km s^{-1}]	σ [km s^{-1}]	χ^2	ł	m	a_s [km s^{-1}]	i [°]	$v \sin i$ [km s^{-1}]	σ [km s^{-1}]
			$f_1 = 5.178964\,\mathrm{d}^{-1}$							$f_3 = 5.066316\,\mathrm{d}^{-1}$			
15.29	1	1	68.7	74.6	46.47	21.00	10.34	1	0	24.8	59.1	42.69	26.23
15.30	1	1	64.9	85.0	38.15	27.82	10.38	1	0	24.2	59.2	42.70	26.23
15.31	1	1	48.2	72.1	43.72	21.64	10.39	1	0	25.0	51.5	42.38	26.24
15.32	1	1	72.3	51.4	36.03	28.62	10.40	1	0	26.4	48.9	42.38	26.35
15.33	1	1	50.9	59.2	42.00	22.58	10.41	1	0	25.7	59.2	43.02	26.41
31.62	1	0	68.4	41.2	30.79	26.66	25.99	1	1	18.0	74.6	43.65	26.70
			$f_2 = 5.3324224\,\mathrm{d}^{-1}$							$f_4 = 5.490133\,\mathrm{d}^{-1}$			
12.36	0	0	41.6	-	43.65	25.17	7.73	2	1	26.2	15.3	40.15	27.23
12.83	0	0	37.0	-	36.66	28.11	7.76	2	1	26.2	12.7	40.16	27.17
13.07	0	0	42.6	-	43.33	25.00	7.77	2	1	26.2	12.7	40.79	26.76
13.53	0	0	33.4	-	40.47	26.41	7.79	2	1	27.1	12.7	40.79	27.11
13.68	0	0	33.3	-	44.60	24.70	7.83	2	1	24.2	12.8	42.38	26.35
							43.68	2	2	23.7	82.4	41.76	26.26

Table 4. Mode parameters derived from the FPF method through a simultaneous fit of the four main modes. We used the same symbol conventions as in Table 3. The 95% significance limit is at $\chi^2 = 1.31$.

χ^2	a_{s1}	a_{s2}	a_{s3}	a_{s4}	i	$v \sin i$	σ
		[km s^{-1}]			[°]	[km s^{-1}]	[km s^{-1}]
			$f_{1;(1,1)}, f_{2;(0,0)}, f_{3;(1,0)}, f_{4;(2,1)}$				
7.26	91.6	54.9	24.5	29.6	43.7	36.7	22.1
7.34	91.6	59.3	26.9	28.8	46.2	37.0	21.6
7.51	98.4	57.4	18.0	28.8	43.7	35.1	22.0
7.55	83.8	51.1	24.5	28.8	54.0	35.4	21.7
7.64	90.6	50.4	26.9	28.8	43.7	37.1	22.1

ble 4). Fig. 7 illustrates the best models for the amplitude and phase across the line profile for the four main modes.

Finally, we tried to identify the other low-amplitude modes with the same methodology and by imposing the wavenumbers (ℓ, m) deduced for the 4 main modes. Unfortunately, we could not obtain additional conclusions. Our failure is not very surprising since these modes have amplitudes lower or of the same order as the harmonics and combination frequencies also present in the signal while nonlinear terms are not taken into account in our line-profile modelling. Fig. 8 depicts the amplitude and phase across the line for these low amplitude modes. Despite the fact that the phase across the profile is well determined for these modes and seems to point to axisymmetric or prograde modes, the χ^2 values between the different options were not discriminative so we do not use that information in the following. In Table 5, we summarize the final outcome of both the photometric (Handler et al. 2006) and spectroscopic mode identifications.

Table 5. Final results for the mode identifications of 12 Lac from our spectroscopic analysis together with the results from the photometric amplitude ratios (Handler et al. 2006).

| ID	Frequency [d^{-1}]	ł Spectr.	Phot.	m
f_1	5.178964	**1**	1	**1**
f_2	5.334224	**0**	0	**0**
f_3	5.066316	**1**	1	**0**
f_4	5.490133	**2**	2	**1**
f_g	0.342841	–	1,2,4	–
f_5	4.241787	–	2	0, 1, 2
f_6	5.218075	–	2,4	–
f_7	6.702318	–	1	–
f_8	7.407162	–	1,2	–
f_9	5.84511	–	1,2	–
f_p	5.30912	–	1,2	–

4.3 Derivation of the surface equatorial rotational velocity and the inclination

From mode identification we can also estimate the inclination, $v \sin i$ and the equatorial rotational velocity v_{eq}. By using χ^2 as a weight we can construct histograms for i, $v \sin i$ and v_{eq}. In Fig. 9 we display these histograms. They are computed by considering all the solutions of the FPF method with the correct wavenumbers of the four dominant modes through a simultaneous fit, and by giving each parameter $(i_k, v \sin i_k$ and $v_{eq,k})$ its appropriate weight $w_k = \chi_0^2/\chi_k^2$, where χ_0^2 is the χ^2-value for the best solution. By calculating a weighted mean and standard deviation of the data, we get $i = 48 \pm 2\,°$, $v \sin i = 36 \pm 2\,\mathrm{km\,s}^{-1}$ and $v_{\mathrm{eq}} = 49 \pm 3\,\mathrm{km\,s}^{-1}$. This leads to a surface rotational frequency between 0.11 and $0.12\,\mathrm{d}^{-1}$ for the appropriate stellar models in Table 6, which will be discussed further on. In the same way we constructed
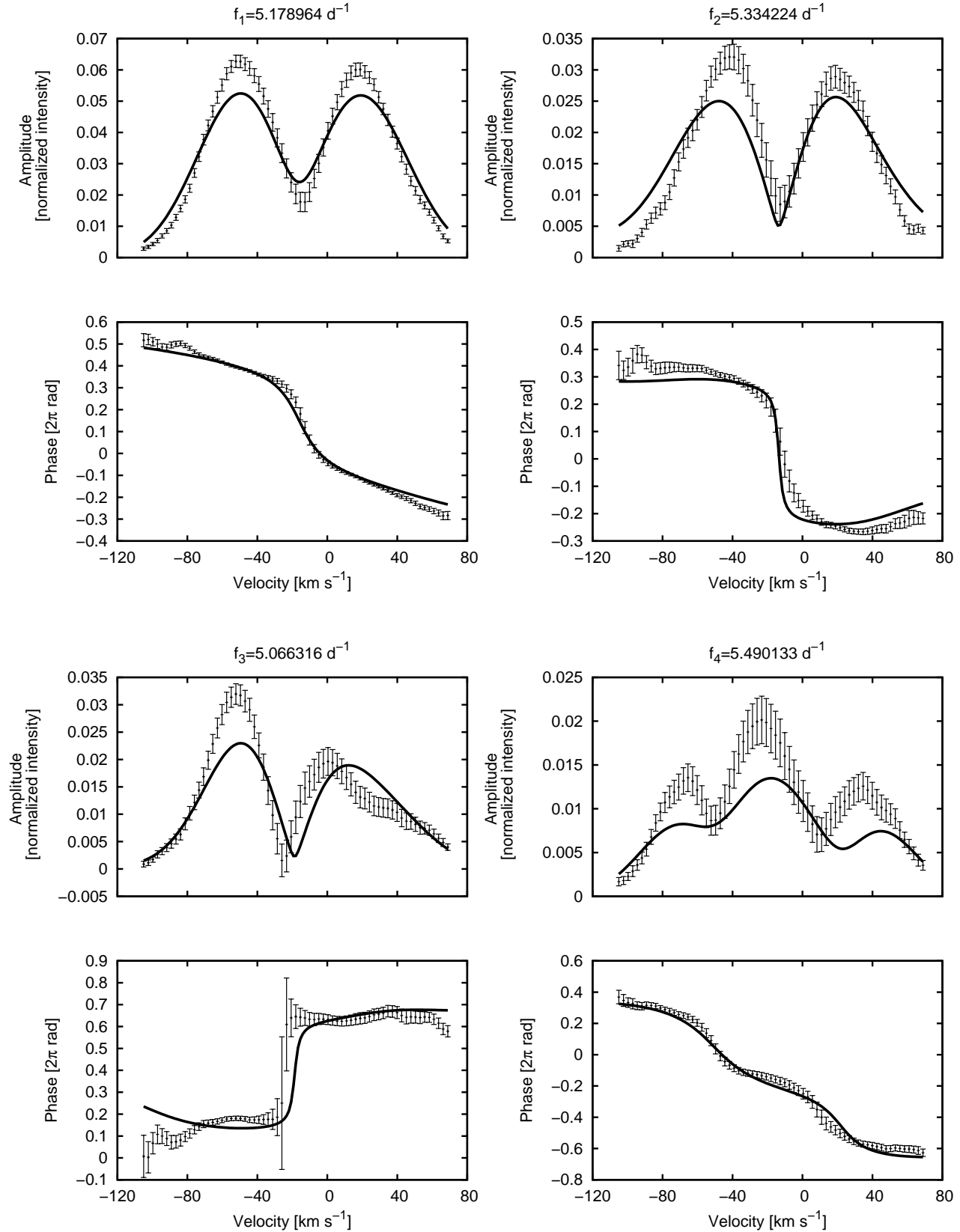
Figure 7. Observed Fourier parameters (black points with error bars) across the line profile together with the best fit for the four identified modes (full line). The amplitudes are expressed in units of continuum and the phases in 2π radians.
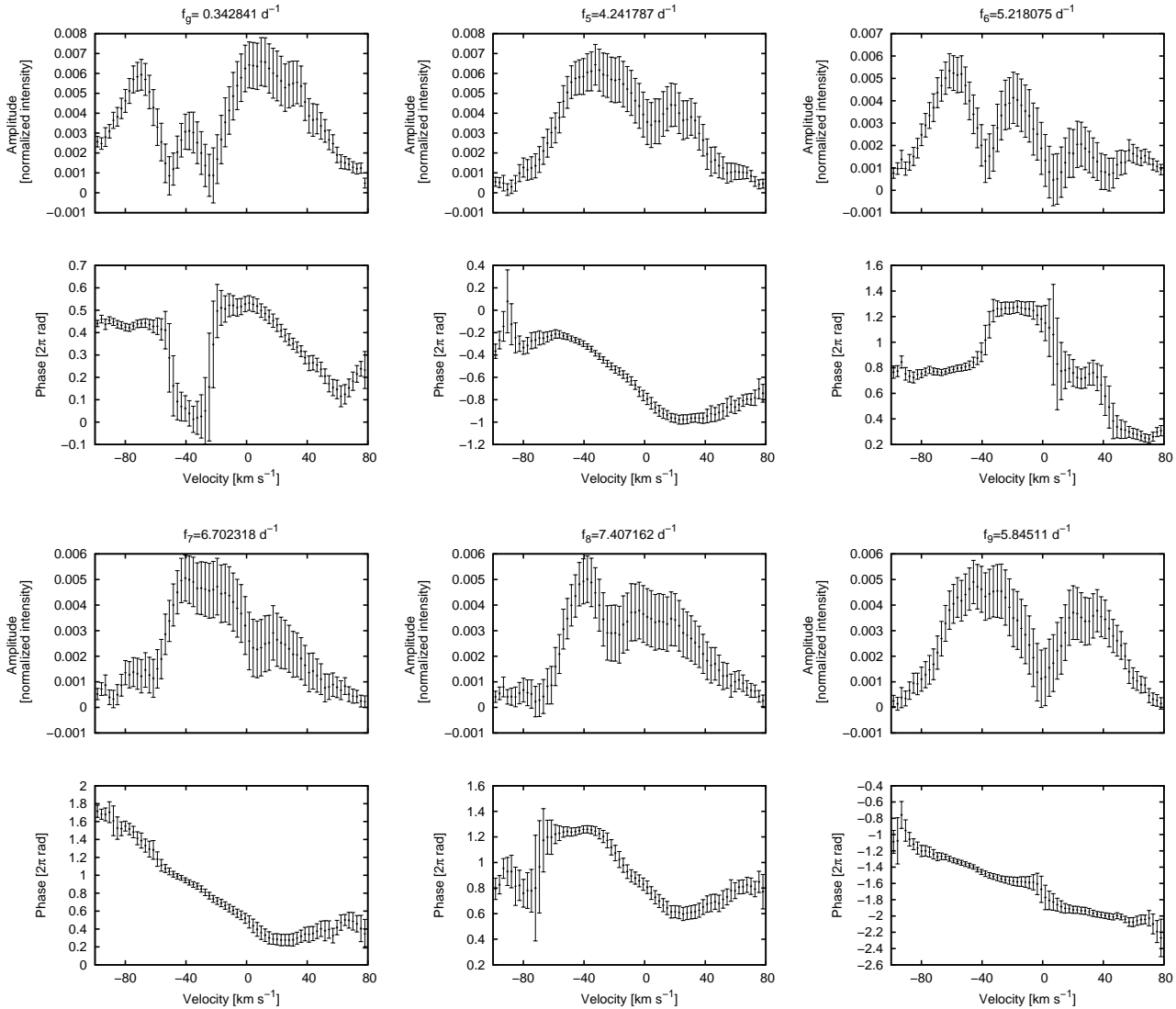
Figure 8. Observed Fourier parameters (black points with error bars) across the line for the detected pulsation frequencies ($f_{g,5-9}$). The amplitudes are expressed in units of continuum and the phase in 2π radians.

these histograms with the solutions from the multi-mode fit of the moment method. However, the moment method did not have the ability to limit the range for i and, by implication, leads to a less trustworthy estimate of v_{eq}. The reason for this is probably that the moment method is based on integrated quantities over the line profile, while in the FPF method we use all the information across the line profile as a whole, which is more sensitive to the position of the nodal lines across the stellar surface and thus to the stellar inclination.

5 MODELLING

In this section, we check if state-of-the-art stellar models with standard physics can account for the observed frequency spectrum together with the derived wavenumbers (ℓ, m) for our studied star. By doing so, we can constrain 12 Lac's model parameters, which are the mass, the central hydrogen abundance and the core con-

vective overshooting parameter. Such asteroseismic constraints have recently been derived for a few β Cephei stars: 16 Lac (Thoul et al. 2003), V836 Cen (Aerts et al. 2003; Dupret et al. 2004), ν Eri (Pamyatnykh et al. 2004; Ausseloos et al. 2004; Dziembowski & Pamyatnykh 2008), δ Ceti (Aerts et al. 2006), β CMa (Mazumdar et al. 2006), θ Oph (Briquet et al. 2007). Finally, Ausseloos (2005) and, more recently, Dziembowski & Pamyatnykh (2008) already made a comparison with stellar models for 12 Lac.

5.1 Numerical tools and physical inputs

In our work, we used the following numerical tools and physical inputs. The stellar models for non-rotating stars were computed with the evolutionary code CLÉS (Code Liégeois d'Évolution Stellaire, Scuflaire et al. 2008b). We used the OPAL2001 equation of state (Rogers & Nayfonov 2002; Caughlan & Fowler 1988), with nuclear reaction rates from Formicola et al. (2007) for the $^{14}\text{N}(p,\gamma)^{15}\text{O}$ cross-
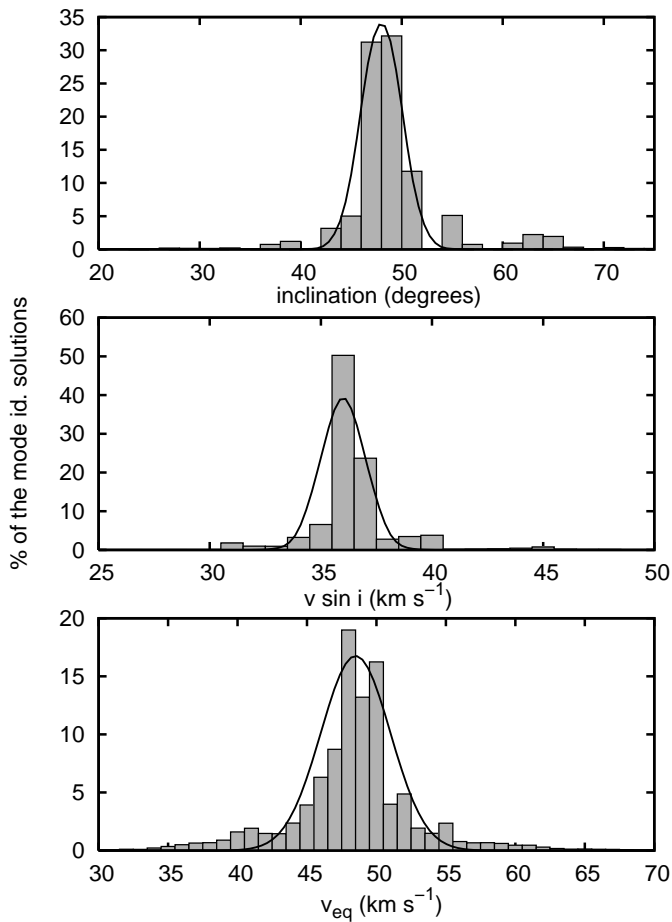
Figure 9. Histograms for the inclination, projected rotation velocity and equatorial rotational velocity of the star derived from the FPF method.

section. Convective transport is treated by using the classical Mixing Length Theory of convection (Böhm-Vitense 1958). For the chemical composition, we used the solar mixture from Asplund et al. (2005). We used OP opacity tables (Seaton 2005) computed for this latter mixture. These tables are completed at $\log T < 4.1$ with the low temperature tables of Ferguson et al. (2005).

Our choice for the metal mixture and the opacities is justified by the following arguments. First, Morel et al. (2006) found that the abundances of He, C, N, O, Mg, Al, Si, S and Fe are, within the errors, in good agreement with the solar values derived from time-dependent, three-dimensional hydrodynamical models of Asplund et al. (2005, and references therein). Secondly, Ausseloos (2005) performed a preliminary seismic study of 12 Lac and was confronted with the problem that, when using OPAL opacities, not all observed pulsation modes can be excited for realistic values of the metallicity and core overshooting parameter. This excitation problem is encountered with the Grevesse et al. (1993) but also with the Asplund et al. (2005) mixture, even for large values of Z (typically larger than 0.016). If we consider values of Z smaller than 0.016, which are more representative of the star, the problem is obviously increased. As discussed in Briquet et al. (2007) for θ Oph, modes that are stable with OPAL opacities (Rogers & Iglesias 1992; Rogers & Nayfonov 2002) can be predicted to be unstable

with OP opacities. The reason is that in a typical β Cephei model the OP opacity is 25% larger than the one for OPAL in the region where the driving of pulsation modes occurs. We consequently wish to check if the use of OP opacity tables improves the situation in the case of the modelling of 12 Lac. We refer to Miglio et al. (2007) for a detailed discussion on the implication of the adopted opacity tables and metal mixtures on the excitation of pulsation modes in the case of B-type stars.

For each stellar model, we calculated the theoretical frequency spectrum of low-order p- and g-modes with a degree of the oscillation up to $\ell = 4$ using a standard adiabatic code for non-rotating stellar models (Scuflaire et al. 2008a), which is much faster than a non-adiabatic code but leads to the same theoretical pulsation frequencies within the adopted precision of the fit, which was 10^{-3} d^{-1}. Once the models fitting the observed modes are selected, we checked the excitation of the pulsation modes with the linear non-adiabatic code MAD developed by Dupret (2001).

5.2 Seismic analysis

Besides the pulsation characteristics summarized in Table 5, we also use $T_{\rm eff}$, $\log g$ and the metallicity Z as additional observational constraints. Geneva photometry of 12 Lac provides $T_{\rm eff} = 23500{\pm}700$ K and $\log g = 3.4{\pm}0.4$ (Handler et al. 2006). From IUE spectra, Niemczura & Daszyńska-Daszkiewicz (2005) derived $T_{\rm eff} = 23600{\pm}1100$ K and $\log g = 3.65 \pm 0.15$. Morel et al. (2006) obtained $T_{\rm eff} = 24\,500{\pm}1000$ K and $\log g = 3.65{\pm}0.1$ from optical spectra. Using another method on the same spectra as Morel et al. (2006), Lefever (2008) deduced $T_{\rm eff} = 24000{\pm}1000$ K and $\log g = 3.60{\pm}0.1$. Morel et al. (2006) also determined a metallicity $Z = 0.0089{\pm}0.0018$.

Stellar models are parametrized by the initial hydrogen abundance X, the core convective overshooting parameter $\alpha_{\rm ov}$, the metallicity Z and the mass M. We adopted $X = 0.72$ but using a different value for X in a reasonable range does not change the conclusions.

We considered two values for Z, i.e. 0.010 and 0.015. The first chosen value corresponds to a metallicity typical of B dwarfs in the solar neighbourhood, also found for 12 Lac within the errors (see above, Morel et al. 2006). The second choice corresponds to the solar composition and the reason for also adopting this value is the following. The star being a relatively slow rotator and its surface convective zone being very thin, diffusion mechanisms can alter the photospheric abundances, leading to Z smaller at the surface compared to the interior of the star. However, since these effects are limited to the very surperficial layers, including a diffusion treatment or not does not affect the derived stellar parameters. It has been carefully checked in the case of θ Oph. We refer to Briquet et al. (2007) for a deeper discussion. For simplicity, we computed non-rotating stellar models without taking into account diffusion, but we also considered a Z higher than what is derived from spectra.

Several values for $\alpha_{\rm ov}$ in the range [0.0-0.5] were tested. The reason is that recent asteroseismic modelling of several β Cephei stars (listed above) showed the occurrence of core overshooting with $\alpha_{\rm ov}$ in the range [0.05-0.25] for all studied stars except θ Oph for which an even higher value of ~ 0.45 was determined. Moreover, other works corroborate the ne-

cessity to include core overshooting in modelling of massive B-type stars. For instance, Deupree (2000) derived a value of about 0.45 by means of 2D hydrodynamic simulations of zero-age main-sequence convective cores. We also mention that, with his study of 13 detached double-lined eclipsing binaries, Claret (2007) found that models with core overshooting of $\alpha_{\mathrm{ov}} \sim 0.2$ are needed to analyse $\sim$10 $M_\odot$ stars.

The observed radial mode with $f_2 = 5.334224\,\mathrm{d}^{-1}$ and the $\ell = 1$ zonal mode with $f_3 = 5.066316\,\mathrm{d}^{-1}$ were selected as the first two frequencies to be confronted with the theoretically predicted frequencies. This was an obvious choice since these are zonal modes ($m = 0$) and thus we do not need any information about the equatorial frequency of rotation to fit them with the model frequencies. We considered two different scenarios: f_2 being either the radial fundamental mode or the first overtone.

The theoretical frequency spectrum with f_2 being the radial fundamental mode is globally compatible with the observed frequencies of 12 Lac. However, all such models fail to reproduce the $\ell = 1$ mode with $f_7 = 6.702318\ \mathrm{d}^{-1}$. If f_2 corresponds to a radial fundamental mode, f_7 can only be an $\ell = 2$ mode according to theoretical models, while the observed photometric amplitude ratios for this mode point out an $\ell = 1$ (Handler et al. 2006). Unfortunately, we cannot confirm this strong constraint since our spectroscopic mode identification was not conclusive for this mode. However, stellar models with f_2 corresponding to the radial first overtone can account for a $\ell = 1$ mode with f_7. We consequently favour a radial order $n = 2$ for f_2. An additional strong argument to favour f_2 as the radial first overtone is the following. The Ledoux rotational splitting is defined by $f_{\mathrm{Ledoux}} = m\beta_{nl}\bar{f}_{\mathrm{rot}}$, where β_{nl} is a structure constant depending on the stellar model, and originates from the frequency splitting defined as

$$f_m = f_0 + m\beta_{nl}\bar{f}_{\mathrm{rot}} = \nu_0 + m\int_0^R K(r)\frac{\Omega(r)}{2\pi}\frac{\mathrm{d}r}{R}, \quad (1)$$

where f_m is the cyclic frequency of a mode of azimuthal-order m, $\Omega(r)$ is the angular velocity, and $K(r)$ is the rotational kernel (for more information, see Scuflaire et al. 2008a). With f_2 as fundamental, the difference between the frequency $f_5 = 4.241787\,\mathrm{d}^{-1}$ and the nearest quadrupole mode (at $\sim$3.8 d^{-1}) is too large to be explained by the Ledoux rotational splitting and thus f_5 cannot be fitted. With f_2 as first overtone, f_5 is easily identified as the g_2 mode with $(\ell, m) = (2, 1)$ as shown below (see also Fig. 11). With f_2 being the first overtone, f_3 is identified as p_1.

The couple (X, Z) being fixed, the fitting of two frequencies suffices to derive the stellar age and stellar mass for adopted α_{ov}. The positions in the $\log(T_{\mathrm{eff}}) - \log g$ diagram of the models matching f_2 and f_3 for different values of α_{ov} are shown in Fig.10. The corresponding parameters are listed in Table 6 for $Z = 0.015$. The mass decreases when the core overshooting parameter increases. We also note the perfect agreement between the $\log g$ of the models and the value deduced from spectroscopic observations. Moreover, the best agreement in T_{eff} corresponds to models with α_{ov} between 0.0 and 0.4 and a mass between 10.0 and 14.4 $M_\odot$. Note that a decrease in Z implies an increase in mass and, considering a Z of 0.010 instead of 0.015 increases the mass by 0.5 $M_\odot$ at most.

Table 6. Physical parameters of the models that match f_2 (being the first overtone) and f_3, with $X = 0.72$ and $Z = 0.015$. X_c is the central hydrogen abundance. The age τ is expressed in million years.

α_{ov}	M $(M_\odot)$	T_{eff} (K)	$\log g$	X_c	R $(R_\odot)$	$\log(L/L_\odot)$	$\tau\,(My)$
0.0	14.4	25600	3.70	0.13	8.8	4.48	11
0.1	13.1	24500	3.68	0.15	8.6	4.38	13
0.2	12.0	23600	3.66	0.17	8.4	4.29	16
0.3	11.0	22750	3.65	0.19	8.2	4.21	20
0.4	10.2	22000	3.64	0.21	8.0	4.13	23
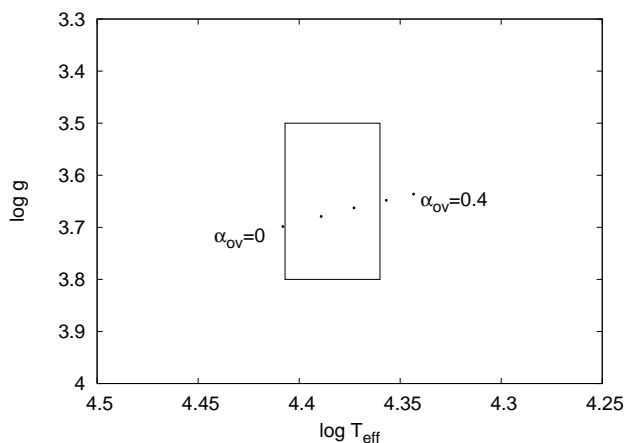
Figure 10. The error box represents the position of 12 Lac in the $\log(T_{\mathrm{eff}}) - \log g$ diagram. The positions of the models which fit exactly f_2 (being the first overtone) and f_3 are also shown for different α_{ov} values.

5.3 Radial order identifications

The frequency $f_1 = 5.178964\,\mathrm{d}^{-1}$ can only belong to the p_1 triplet. The frequency splitting $f_1 - f_3$ is 0.1126 d^{-1}. According to the models, $\beta_{nl} = 0.5$ for this mode. This yields an averaged frequency of rotation $\bar{f}_{\mathrm{rot}} = (f_1 - f_3)/m\beta_{nl}$. This averaged rotation frequency leads to a rotational velocity twice as high as the surface value estimated from our spectroscopic observations (with corresponding velocities of $100\,\mathrm{km\,s}^{-1}$ versus $49\,\mathrm{km\,s}^{-1}$). We thus confirm that 12 Lac must rotate more rapidly in its inner parts than at the surface, as already emphasized by Dziembowski & Pamyatnykh (2008).

As can be seen in Fig. 11, the $(\ell = 1, p_3)$ mode can account for $f_7 = 6.702318\,\mathrm{d}^{-1}$. The match is not perfect for all models in Table 6. This is probably due to the fact that there can occur small shifts due to rotation. On the other hand a change in metallicity will also cause a small shift of the theoretical frequencies (see Sect. 5.5). The frequency $f_8 = 7.407162\,\mathrm{d}^{-1}$ and $f_9 = 5.84511\,\mathrm{d}^{-1}$ can only be the $(\ell = 2, p_2)$ mode and the $(\ell = 1, p_2)$ mode, respectively. Indeed, no theoretical frequency of an $\ell = 1$ zonal mode and an $\ell = 2$ zonal mode is in the vicinity of f_8 and f_9, respectively. We also note that an $l = 0$ radial-mode solution for f_8 is excluded (see Table 5).

The frequency $f_p = 5.30912\,\mathrm{d}^{-1}$ found in photometry

Table 7. The ℓ, n and m identifications according to our mode identification and modelling with the radial mode as first overtone. We use the usual convention that negative n-values denote g-modes (see e.g. Unno et al. 1989).

ID	Frequency [d^{-1}]	ℓ	n	m
f_1	5.178964	1	1	1
f_2	5.334224	0	2	0
f_3	5.066316	1	1	0
f_4	5.490133	2	0	1
f_5	4.241787	2	-2	1
f_6	5.218075	4	-2 or -1	
f_7	6.702318	1	3	
f_8	7.407162	2	2	
f_9	5.84511	1	2	
f_p	5.30912	2	0	0

and the frequency $f_4 = 5.490133\,\mathrm{d}^{-1}$ were both identified as quadrupole modes and can be accounted for by the $(\ell = 2, f)$ mode. Indeed, the theoretical Ledoux frequency splitting assuming the averaged internal rotation frequency value $\bar{f}_{\mathrm{rot}}$ derived from $f_1 - f_3$ ranges in $[0.186\text{-}0.190]\,\mathrm{d}^{-1}$ for different overshooting values, which corresponds to the difference between f_p and f_4. The frequency f_p thus corresponds to $(\ell, m) = (2, 0)$ and f_4 to $(\ell, m) = (2, 1)$ in accordance with the $m-$identification for f_4. Note that the theoretical frequency value for the $(\ell = 2, f)$ mode is in best agreement for $\alpha_{\mathrm{ov}} = 0.0$ and is $5.287\,\mathrm{d}^{-1}$.

$f_5 = 4.241787\,\mathrm{d}^{-1}$ being a prograde $\ell = 2$ mode, is uniquely identified as the $(\ell = 2, \mathrm{g}_2)$ mode. The corresponding theoretical zonal mode has a frequency between 4.048 and 4.070 d^{-1} with a Ledoux splitting for that mode ranging between 0.183 and 0.185 d^{-1} deduced from $\bar{f}_{\mathrm{rot}}$ and $\beta_{nl} = 0.80$. In addition, we thus conclude that $m = 1$ for this mode.

$f_6 = 5.218075\,\mathrm{d}^{-1}$ may be either identified as $(\ell = 4, \mathrm{g}_2)$ or $(\ell = 4, \mathrm{g}_1)$ (see also Fig. 11). The models give $\beta_{nl} = 0.97$ for this mode. In the first case, the zonal frequency ranges between 4.38 and 4.55 d^{-1} with a Ledoux splitting of 0.21-0.22 d^{-1} deduced from $\bar{f}_{\mathrm{rot}}$. This corresponds to an m-value of 3 or 4. In the second case, the zonal frequency ranges between 5.57 and 5.70 d^{-1} with a Ledoux splitting of 0.20-0.21 d^{-1}. This corresponds to an m-value of -2.

Finally, nothing can be concluded for $f_g = 0.342841\,\mathrm{d}^{-1}$ because of the dense theoretical frequency spectrum in the low-frequency range and because of the lack of observed constraints on the wavenumbers of this mode. We additionally note that we cannot definitely exclude this frequency to be linked with the frequency of rotation. For instance, $f_g/3$ is compatible with our observed surface equatorial rotation frequency. As explained in Briquet et al. (2001, 2004), one way to discriminate between the pulsation and rotation interpretation is to compare the variability of the considered frequency in lines of different chemical elements. Unfortunately, we could not achieve such a test because lines other than Si lines are at our disposal only for two nights of observation. This time span is not long enough to recover such a low frequency value.

Table 8. Observed photometric amplitude ratios taken from Handler et al. (2006). We also list our best fitting theoretical amplitude ratios. They originate from the model with $\alpha_{\mathrm{ov}} = 0.4$ given in Table 6.

| ID	Frequency [d^{-1}]	v/u obs.	v/u theory	V/u obs.	V/u theory
f_2	5.334224	0.529(7)	0.64	0.456(7)	0.56
f_3	5.066316	0.716(8)	0.73	0.686(8)	0.67
f_4	5.490133	0.82(1)	0.83	0.78(1)	0.78

5.4 Comparison with photometry

We used our best models listed in Table 6 to compare our results with the photometric mode identification of Handler et al. (2006). We computed theoretical photometric amplitude ratios for our three main identified pulsation modes (f_2, f_3, f_4; f_1 belongs to f_3) following Dupret et al. (2003). We computed the amplitude ratios for Strömgren u and v, and for Johnson V. For this computation we must determine the nonadiabatic pulsation mode parameters f_T and f_g, where f_T corresponds to the local effective temperature variation and f_g corresponds to the local effective gravity variation, both at the level of the photosphere. We used the non-adiabatic code MAD (Dupret 2001) to compute these $f_{T,g}$ parameters for our best seismic models of 12 Lac.

We list the observed and theoretical photometric amplitudes for the three main modes in Table 8. We refer to Fig. 4 of Handler et al. (2006) for the results of the photometric mode identification. For all the models, we observed that the amplitude ratios decrease with decreasing mass. For f_2 we find amplitude ratios for v/u ranging from 0.68 until 0.64, and for V/u ranging from 0.51 until 0.56. Thus, we encounter exactly the same problem as Handler et al. (2006), i.e., we could not find an perfect agreement for the observed ratios of f_2. For f_3 we find amplitude ratios for v/u ranging from 0.84 until 0.73, and for V/u ranging from 0.74 until 0.67. Our models give amplitude ratios for f_4 for v/u ranging from 0.90 until 0.83, and for V/u ranging from 0.84 until 0.78. Our conclusion is that we can reproduce the observed photometric amplitude ratios for the two main modes (f_3 and f_4) from our best seismic models. Moreover, from this *a posteriori* consistency check, we favour a the more evolved seismic models, i.e., those with lower mass and higher core overshoot (see Tables 6 and 8).

5.5 Discussion

We have shown that adopting $n = 2$ for the radial mode cannot be excluded as was done by Dziembowski & Pamyatnykh (2008), and, in fact, explains all observed frequencies according to their photometric and spectroscopic mode identification except for f_g. The identifications of the radial order together with the additional ℓ identifications are summarized in Table 7. A perfect agreement in frequency values is not achieved. One reason might be that slightly different values for (X, Z) than those adopted could lead to a better agreement. Another one may be that small frequency shifts due to rotation may occur as already pointed out by Dziembowski & Pamyatnykh (2008),
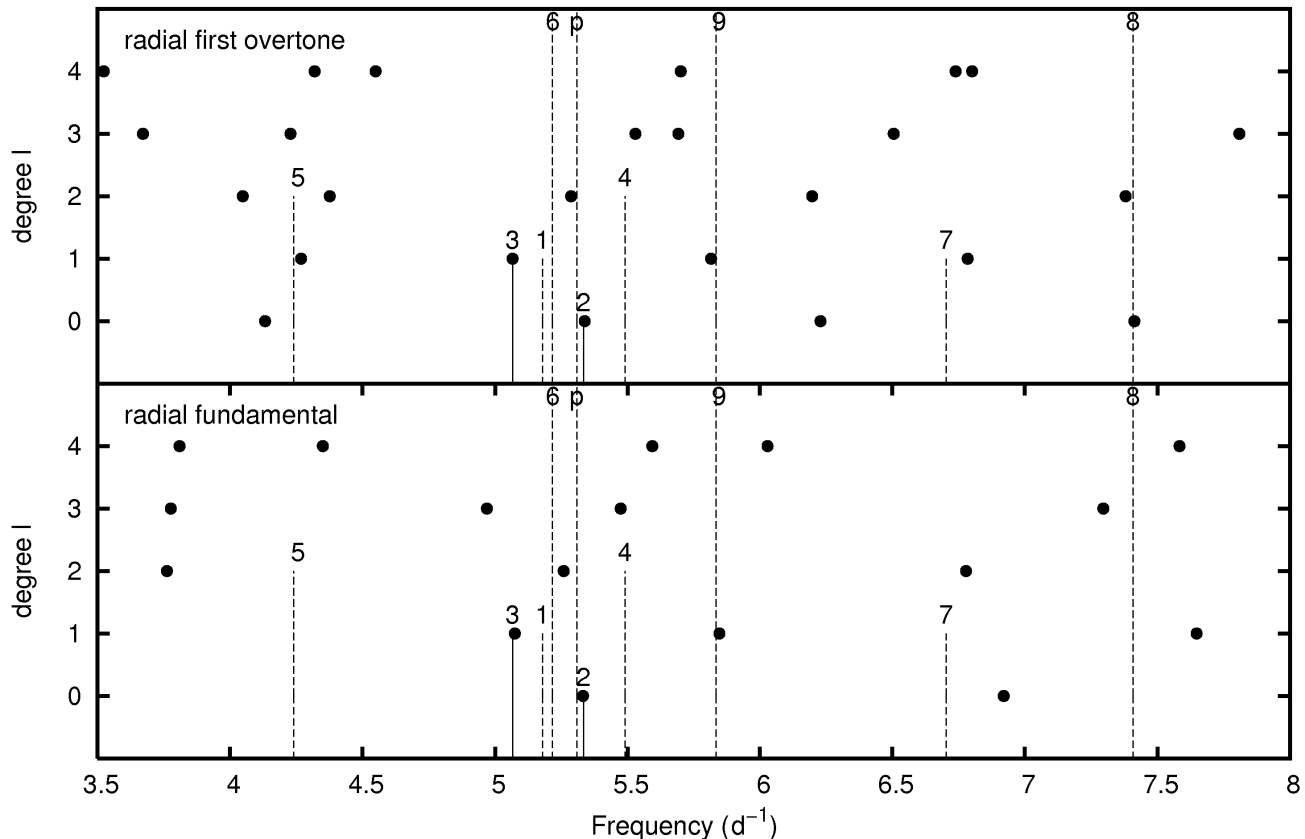
Figure 11. Comparison between the theoretical frequencies ($m = 0$, dots) and the observed frequencies (full and dotted lines) labeled with their frequency identifications as listed in Table 5. The full lines correspond to the two axisymmetric modes f_2 and f_3. The top and bottom panels correspond to f_2 as the radial first overtone and the radial fundamental, respectively. The theoretical models are calculated for $X = 0.72$, $Z = 0.015$ and $\alpha_{\rm ov} = 0.0$.

although the surface equatorial rotation frequency is only a few percent of the measured oscillation frequencies. We found evidence for some degree of differential rotation from the observed splitting between f_1 and f_3. Using the Ledoux splitting, all the other detected frequencies can be well fitted with one and the same averaged rotation frequency $\bar{f}_{\rm rot}$ inside the star, where $\bar{f}_{\rm rot}$ is derived from the model fitting of f_1 and f_3. In the absence of the observations of multiplets we do not have enough constraints to derive the internal rotation profile as defined in Equation (1) and, consequently, to determine its effects on the frequencies and frequency splittings.

Dziembowski & Pamyatnykh (2008) partly included rotation effects in their modelling and proposed a model with the angular rotation velocity more than 4 times higher in the centre of the star compared to the surface. They imposed that the radial mode is the fundamental without considering alternative identifications. Consequently, they could not account for an $\ell = 1$ for f_7. As our results are the same than theirs under the assumption of the radial fundamental mode, we refer to their paper for the properties of the resulting seismic model in this case without repeating it here (see in particular their Fig. 7 and our Fig. 11). Their

assumption of non-rigid rotation is based on the fact that f_5 cannot be fitted because the closest $\ell = 2$ mode is too far to be explained by the splitting due to a uniform rotation. We recall that, on the contrary, our models reproduce the $\ell = 1$ for f_7 and the Ledoux splitting for $\bar{f}_{\rm rot}$ can explain f_5 as the $(\ell, m, n) = (2, 1, -2)$ mode. As additional argument to non-rigid rotation, Dziembowski & Pamyatnykh (2008) stated that their model with uniform rotation has no identification for f_6. We can explain it as the $(\ell = 4, {\rm g}_2)$ mode or the $(\ell = 4, {\rm g}_1)$ mode in agreement with the photometric ℓ-identification. Finally, even with a non-uniform rotation, they cannot reproduce f_5 appropriately while they used this frequency value to exclude rigid rotation.

Until now, the only convincing proof of non-rigid rotation has been achieved for $V836$ Cen (Aerts et al. 2003; Dupret et al. 2004) and for ν Eri (Pamyatnykh et al. 2004; Dziembowski & Pamyatnykh 2008). The only other star with two observed multiplets is θ Oph for which the observed rotational splittings cannot rule out a rigid rotation model. For 12 Lac, we are able to fit the observed frequency spectrum using non-rotating stellar models and Ledoux splittings based on one consistent value $\bar{f}_{\rm rot}$ for the averaged internal rotation frequency derived from the splitting between

f_1 and f_3. The deviation between the rotation frequency derived from fitting the splitting $f_1 - f_3$ and from the observed surface rotation frequency points to some degree of non-rigidity. With only two components of one and the same multiplet observed, we are not able to quantify this statement.

Besides our basic stellar modelling, we also checked if non-adiabatic computations are able to reproduce the excitation of the observed frequencies. Indeed, recent works revealed shortcomings in the details of the excitation mechanism for these massive B-type pulsating stars. For instance, for ν Eri (Pamyatnykh et al. 2004; Ausseloos et al. 2004), the observed lowest g-mode and highest p-mode frequencies were not predicted to be excited by standard models. The same conclusion is found for 12 Lac. Neither the frequency f_g nor the highest p-mode frequencies (f_7 and f_8) are excited by current models, even with OP opacity tables. Since 1991, the agreement between the non-adiabatic computations for β Cephei models and the observations has improved with subsequent update of opacities (see e.g. Miglio et al. 2007; Miglio 2007). Consequently, a most probable explanation for the encountered excitation problem is that current opacities are still underestimated in the region where the driving of pulsation modes occurs. We refer to Dziembowski & Pamyatnykh (2008) for an additional discussion on this matter.

6 CONCLUSIONS

Our study was based on 1820 ground-based, high-resolution, high-S/N, multisite spectroscopic measurements spread over 14 years. As pointed out in Handler et al. (2006) this effort was necessary to identify the previously unknown azimuthal order of the pulsation modes and thus to be able to perform a detailed seismic modelling of the star. We used the Si III 4553 Å line to derive the pulsation characteristics of 12 Lac. In total we find 10 independent frequencies which were also detected in photometry. Worth mentioning is that we also clearly recover the low-frequency signal. One of our aims was to provide a unique identification of as many modes as possible for 12 Lac. The important result of combining our spectroscopic results with the ones from the intensive photometric campaign (Handler et al. 2006) is the unique identification of both ł and m of the four highest-amplitude modes.

With two state-of-the-art methods, the moment method and the FPF method, we were able to identify the azimuthal order of the four main modes. We could also give a constraint on the azimuthal order of the fifth frequency. Two main frequencies were identified as axisymmetric modes. One of which has an ł value of 1 (f_3), the other one is a radial mode (f_2). The two other main frequencies are identified as $(l_1, m_1) = (1, 1)$ and $(l_4, m_4) = (2, 1)$. The conclusion for the fifth frequency is that the azimuthal order is likely to be positive. In addition, the FPF method could also constrain the inclination, $i = 48 \pm 2\,^\circ$, and the surface equatorial rotational velocity, $v_{eq} = 49 \pm 2\,\mathrm{km\,s^{-1}}$.

The definite identification of four of the observed modes together with some constraints of the wavenumbers (either ℓ-values or sign of m) on the other modes allowed us to carry out a detailed seismic modelling, under the assumption of linear oscillation modes. The most significant outcome of our modelling is the fact that there is a strong preference that the observed radial mode (f_2) is the radial first overtone. If f_2 is taken as the radial fundamental, the frequency spectrum of 12 Lac cannot be reproduced satisfactorily. We do point out that the theory we used, as well as Dziembowski & Pamyatnykh (2008), does not include non-linear effects, while these may be present in 12 Lac (e.g. Mathias et al. 1992). It remains to be studied how these would effect mode identification and seismic modelling, but given the very moderate effect and the limit to only very few third-order combination frequencies, we do not expect this to alter our conclusions, just as for the case of ν Eri, where a linear theory was also used (Pamyatnykh et al. 2004).

The complete frequency spectrum of 12 Lac, except the low frequency, can be fully identified. Our seismic modelling also revealed an excitation problem. Indeed, the range of frequencies theoretically excited is not large enough compared to the observations. This might reflect the fact that opacities are still underestimated in the region where the driving of pulsation modes occurs. This conclusion is valid for both the OPAL and OP opacities.

Finally, our best-fit models indicate that the overshooting parameter α_{ov} has to be lower than 0.4 local pressure scale heights to get the best agreement with physical parameters derived from spectroscopic observations. A more refined seismic modelling requires the computation of a much denser grid of models and will be done in future work.

REFERENCES

Aerts C., De Cat P., 2003, Space Science Reviews, 105, 453
Aerts C., De Cat P., Handler G., Heiter U., Balona L. A., Krzesinski J., Mathias P., Lehmann H., Ilyin I., De Ridder J., Dreizler S., Bruch A., Traulsen I., Hoffmann A., James D., Romero-Colmenero E., Maas T., Groenewegen M. A. T., Telting J. H., Uytterhoeven K., Koen C., Cottrell P. L., Bentley J., Wright D. J., Cuypers J., 2004, MNRAS, 347, 463
Aerts C., de Pauw M., Waelkens C., 1992, A&A, 266, 294
Aerts C., Marchenko S. V., Matthews J. M., Kuschnig R., Guenther D. B., Moffat A. F. J., Rucinski S. M., Sasselov D., Walker G. A. H., Weiss W. W., 2006, ApJ, 642, 470
Aerts C., Thoul A., Daszyńska J., Scuflaire R., Waelkens C., Dupret M. A., Niemczura E., Noels A., 2003, Science, 300, 1926

Asplund M., Grevesse N., Sauval A. J., 2005, in Astronomical Society of the Pacific Conference Series, Vol. 336, Cosmic Abundances as Records of Stellar Evolution and Nucleosynthesis, Barnes III T. G., Bash F. N., eds., pp. 25–+

Ausseloos M., 2005, PhD thesis, KULeuven, Belgium

Ausseloos M., Scuflaire R., Thoul A., Aerts C., 2004, MNRAS, 355, 352

Balona L. A., James D. J., Motsoasele P., Nombexeza B., Ramnath A., van Dyk J., 2002, MNRAS, 333, 952

Böhm-Vitense E., 1958, Zeitschrift fur Astrophysik, 46, 108

Breger M., Handler G., Garrido R., Audard N., Zima W., Paparó M., Beichbuchner F., Zhi-Ping L., Shi-Yang J., Zong-Li L., Ai-Ying Z., Pikall H., Stankov A., Guzik J. A., Sperl M., Krzesinski J., Ogloza W., Pajdosz G., Zola S., Thomassen T., Solheim J.-E., Serkowitsch E., Reegen P., Rumpf T., Schmalwieser A., Montgomery M. H., 1999, A&A, 349, 225

Breger M., Stich J., Garrido R., Martin B., Jiang S. Y., Li Z. P., Hube D. P., Ostermann W., Paparo M., Scheck M., 1993, A&A, 271, 482

Briquet M., Aerts C., 2003, A&A, 398, 687

Briquet M., Aerts C., Lüftinger T., De Cat P., Piskunov N. E., Scuflaire R., 2004, A&A, 413, 273

Briquet M., De Cat P., Aerts C., Scuflaire R., 2001, A&A, 380, 177

Briquet M., Lefever K., Uytterhoeven K., Aerts C., 2005, MNRAS, 362, 619

Briquet M., Morel T., Thoul A., Scuflaire R., Miglio A., Montalbán J., Dupret M.-A., Aerts C., 2007, MNRAS, 381, 1482

Caughlan G. R., Fowler W. A., 1988, Atomic Data and Nuclear Data Tables, 40, 283

Claret A., 2007, A&A, 475, 1019

De Cat P., Aerts C., 2002, A&A, 393, 965

De Ridder J., Dupret M.-A., Neuforge C., Aerts C., 2002, A&A, 385, 572

Deupree R. G., 2000, ApJ, 543, 395

Dupret M. A., 2001, A&A, 366, 166

Dupret M.-A., De Ridder J., De Cat P., Aerts C., Scuflaire R., Noels A., Thoul A., 2003, A&A, 398, 677

Dupret M.-A., Thoul A., Scuflaire R., Daszyńska-Daszkiewicz J., Aerts C., Bourge P.-O., Waelkens C., Noels A., 2004, A&A, 415, 251

Dziembowski W. A., Jerzykiewicz M., 1999, A&A, 341, 480

Dziembowski W. A., Pamyatnykh A. A., 2008, MNRAS, 385, 2061

Ferguson J. W., Alexander D. R., Allard F., Barman T., Bodnarik J. G., Hauschildt P. H., Heffner-Wong A., Tamanai A., 2005, ApJ, 623, 585

Formicola A., Imbriani G., Costantini H., Angulo C., Bemmerer D., Bonetti R., Broggini C., Corvisiero P., Cruz J., Descouvemont P., Fulop Z., Gervino G., Guglielmetti A., Gustavino C., Gyurky G., Jesus A. P., Junker M., Lemut A., Menegazzo R., Prati P., Roca V., Rolfs C., Romano M., Rossi Alvarez C., Schumann F., Somorjai E., Straniero O., Strieder F., Terrasi F., Trautvetter H. P., Vomiero A., Zavatar elli S., 2007, Physics Letters B, 591, 61

Grevesse N., Noels A., Sauval A. J., 1993, A&A, 271, 587

Handler G., Jerzykiewicz M., Rodríguez E., Uytterhoeven K., Amado P. J., Dorokhova T. N., Dorokhov N. I., Poretti E., Sareyan J.-P., Parrao L., Lorenz D., Zsuffa D., Drummond R., Daszyńska-Daszkiewicz J., Verhoelst T., De Ridder J., Acke B., Bourge P.-O., Movchan A. I., Garrido R., Paparó M., Sahin T., Antoci V., Udovichenko S. N., Csorba K., Crowe R., Berkey B., Stewart S., Terry D., Mkrtichian D. E., Aerts C., 2006, MNRAS, 365, 327

Handler G., Shobbrook R. R., Jerzykiewicz M., Krisciunas K., Tshenye T., Rodríguez E., Costa V., Zhou A.-Y., Medupe R., Phorah W. M., Garrido R., Amado P. J., Paparó M., Zsuffa D., Ramokgali L., Crowe R., Purves N., Avila R., Knight R., Brassfield E., Kilmartin P. M., Cottrell P. L., 2004, MNRAS, 347, 454

Lefever K., 2008, PhD thesis, KULeuven, Belgium

Lenz P., Breger M., 2005, Communications in Asteroseismology, 146, 53

Mathias P., Aerts C., Gillet D., Waelkens C., 1994, A&A, 289, 875

Mathias P., Gillet D., Crowe R., 1992, A&A, 257, 681

Mazumdar A., Briquet M., Desmet M., Aerts C., 2006, A&A, 459, 589

Miglio A., 2007, PhD thesis, Université de Liège, Belgium

Miglio A., Montalbán J., Dupret M.-A., 2007, MNRAS, 375, L21

Montgomery M. H., O'Donoghue D., 1999, Delta Scuti Star Newsletter, 13, 28

Morel T., Butler K., Aerts C., Neiner C., Briquet M., 2006, A&A, 457, 651

Niemczura E., Daszyńska-Daszkiewicz J., 2005, A&A, 433, 659

Pamyatnykh A. A., 1999, Acta Astronomica, 49, 119

Pamyatnykh A. A., Handler G., Dziembowski W. A., 2004, MNRAS, 350, 1022

Rogers F. J., Iglesias C. A., 1992, ApJS, 79, 507

Rogers F. J., Nayfonov A., 2002, ApJ, 576, 1064

Schrijvers C., Telting J. H., 1999, A&A, 342, 453

Schrijvers C., Telting J. H., Aerts C., 2004, A&A, 416, 1069

Scuflaire R., Montalbán J., Théado S., Bourge P.-O., Miglio A., Godart M., Thoul A., Noels A., 2008a, Ap&SS, 316, 149

Scuflaire R., Théado S., Montalbán J., Miglio A., Bourge P.-O., Godart M., Thoul A., Noels A., 2008b, Ap&SS, 316, 83

Seaton M. J., 2005, MNRAS, 362, L1

Stankov A., Handler G., 2005, VizieR Online Data Catalog, 215, 80193

Telting J. H., Aerts C., Mathias P., 1997, A&A, 322, 493

Thoul A., Aerts C., Dupret M. A., Scuflaire R., Korotin S. A., Egorova I. A., Andrievsky S. M., Lehmann H., Briquet M., De Ridder J., Noels A., 2003, A&A, 406, 287

Unno W., Osaki Y., Ando H., Saio H., Shibahashi H., 1989, Nonradial oscillations of stars. Nonradial oscillations of stars, Tokyo: University of Tokyo Press, 1989, 2nd ed.

Wilson R. E., 1953, Carnegie Institute Washington D.C. Publication, 0

Zima W., 2006, A&A, 455, 227

—, 2008, Communications in Asteroseismology, 155, 1

Zima W., Kolenberg K., Briquet M., Breger M., 2004, Communications in Asteroseismology, 144, 5

This paper has been typeset from a TEX/ LATEX file prepared by the author.